# Electronic Supplementary Material

# Cobalt-nitrogen co-doped porous carbon sphere as highly efficient catalyst for liquid-phase cyclohexane oxidation with molecular oxygen and the active sites investigation

Lei Chen, Yuan Sun, Jinshan Chi, Wei Xiong (✉), Pingle Liu, Fang Hao (✉)

College of Chemical Engineering, National & Local United Engineering Research Centre for Chemical Process Simulation and Intensification, Xiangtan University, Xiangtan 411105, China

E-mails: haofang.happy@163.com (Hao F); happy.xiongw@163.com (Xiong W)

## S1 Computational Details

### *S1.1 Calculation methods*

All density function (DFT) calculation was carried out using the DMol$^3$ package in Material Studio software. The electronic exchange and correlation energies were calculated by using Generalized Gradient Approximation (GGA) in the Perdew-Burke-Ernzerhof (PBE) parametrization. The valence electron functions were expanded by the adoption of the Double Numerical plus d-functions (DND) basis set, and the inner electrons of atoms were frozen and represented by the density-functional semi-core pseudopotentials (dspp). All atoms were fully relaxed and optimized, and the convergence criteria of energy, force, and displacement were set to $2.0 \times 10^{-5}$ Ha (1 Ha = 27.2114 eV), $4.0 \times 10^{-3}$ Ha·Å$^{-1}$, and $5.0 \times 10^{-3}$ Å, respectively. For the energy calculations of the N-doped graphene with 6×8×1 supercell and $Co_4$ nanocluster, the Brillouin zone was sampled using a Monkhorst-Pack scheme with a 2×2×1 k-point grid. To determine the transition state structure, the complete linear and quadratic synchronous transit (LST/QST) method was applied. The nature of the minima and transition states of the reaction path was checked by calculating the harmonic vibration frequencies.

## Tables and Figures

**Table S1. The textural properties of the catalysts**

| Catalysts | BET surface area ($m^2$ $g^{-1}$) | Pore size (nm) | Pore volume ($cm^3$ $g^{-1}$) |
|---|---|---|---|
| Co-NC-0 | 264.36 | 4.23 | 0.19 |
| Co-NC-0.5 | 350.47 | 5.91 | 0.32 |
| Co-NC-1 | 305.06 | 4.21 | 0.22 |
| Co-NC-2 | 306.10 | 4.34 | 0.26 |
| Co-NC-4 | 385.94 | 4.65 | 0.25 |

**Table S2. The chemical composition of different elements over the prepared catalysts obtained by XPS analysis**

| Catalysts | Co | Different Co Con. % | | | N | Different N Con. % | | | | O | C |
|---|---|---|---|---|---|---|---|---|---|---|---|
| | % | $Co^0$ | $Co^{3+}$ | Co-N | % | $N_{pyri}$ | $N_{pyrr}$ | $N_{grap}$ | $N_{oxid}$ | % | % |
| Co-NC-0 | 0.7 | 26.8 | 43.0 | 30.2 | 3.5 | 16.6 | 40.7 | 27.5 | 15.2 | 0.2 | 95.6 |
| Co-NC-2 | 1.1 | 46.7 | 32.5 | 20.8 | 3.3 | 33.2 | 19.7 | 33.0 | 14.1 | 3.1 | 92.5 |

$N_{pyri}$: pyridine-N, $N_{pyrr}$: pyrrolic-N, $N_{grap}$: graphitic-N, $N_{oxid}$: oxidized-N

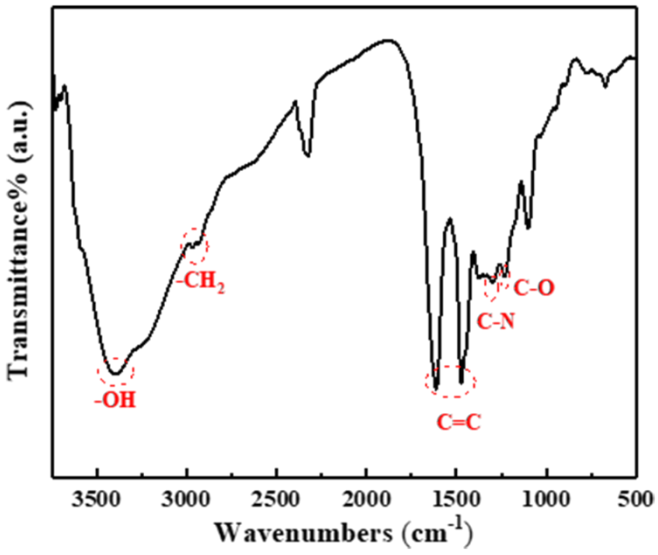


**Figure. S1. FT-IR spectra of RF resin microspheres.**

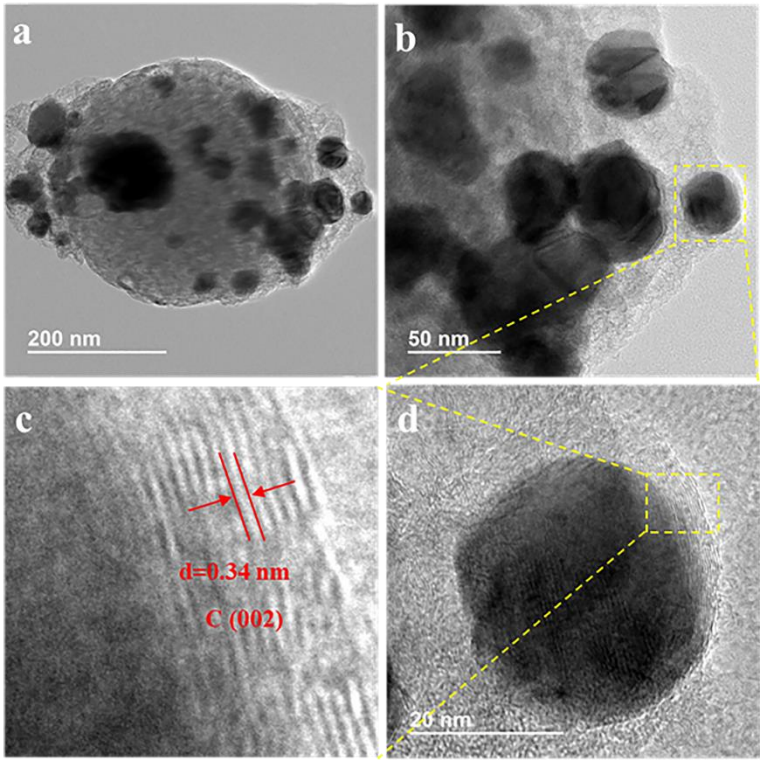


**Figure. S2. TEM images of the Co-NC-0.**

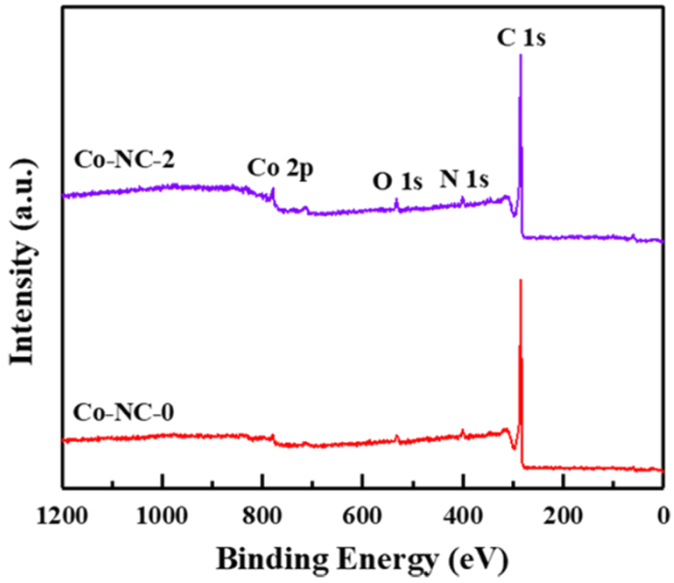


**Figure S3. XPS full spectrum of Co-NC-0 and Co-NC-2.**

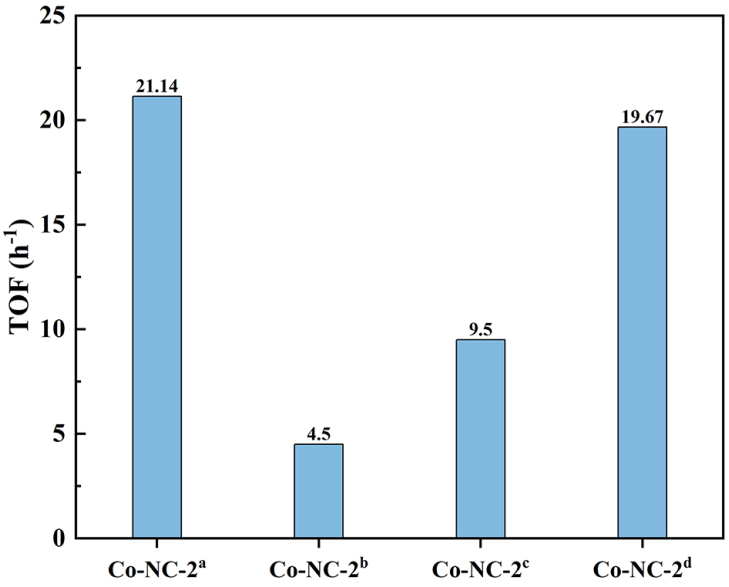


**Figure S4. Turnover frequencies (TOF) of Co-NC-2 prepared by different methods in liquid phase selective oxidation of cyclohexane: (a) ultrasonic-assisted method, (b) Room temperature stirring method; (c) Hydrothermal method; (d) Zn-Co-ZIF derived Co-NC.**

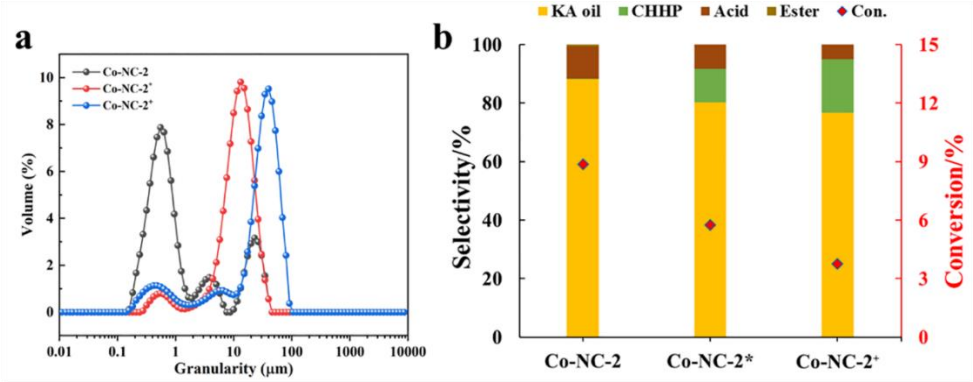


**Figure S5. The particle size distribution of different Co-NC-2 samples and catalytic performance for the selectivity oxidation of cyclohexane.**

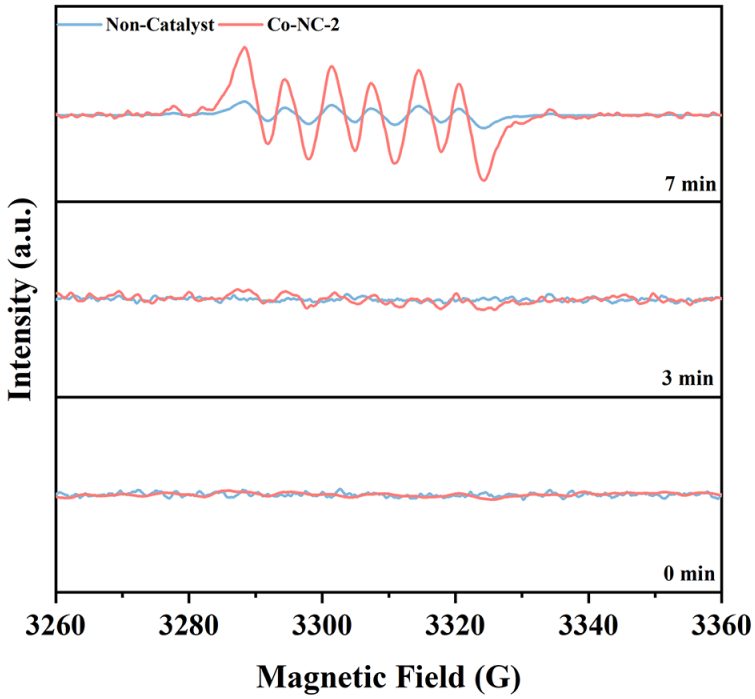


**Figure S6. EPR spectra for the mixture of $C_6H_{12}$, and DMPO with $O_2$ atmosphere at time intervals of 0, 3, and 7 min.**

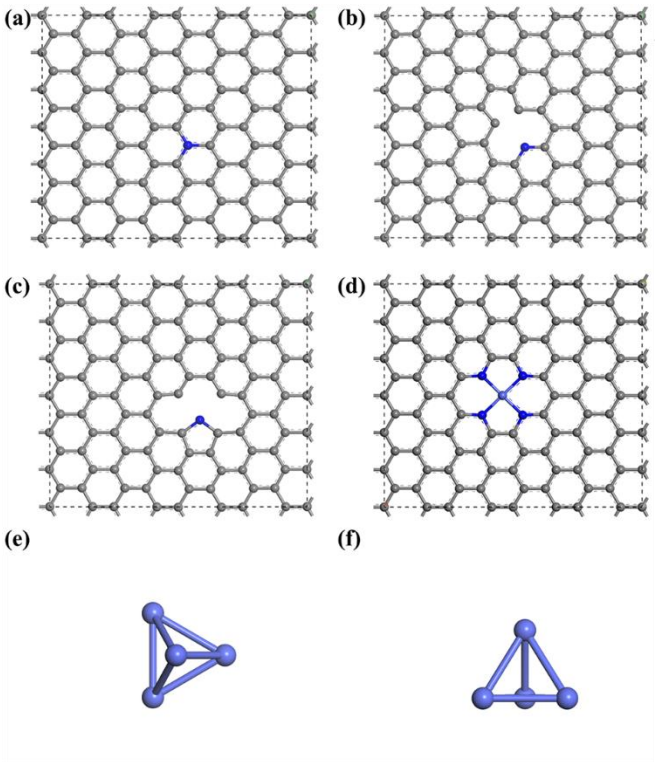


**Figure S7. Top view of the atomic structures of (a) graphitic-N, (b) pyridinic-N, (c) pyrrolic-N, (d) Co-N-C, (e) $Co_4$, and side view of (f) $Co_4$.**

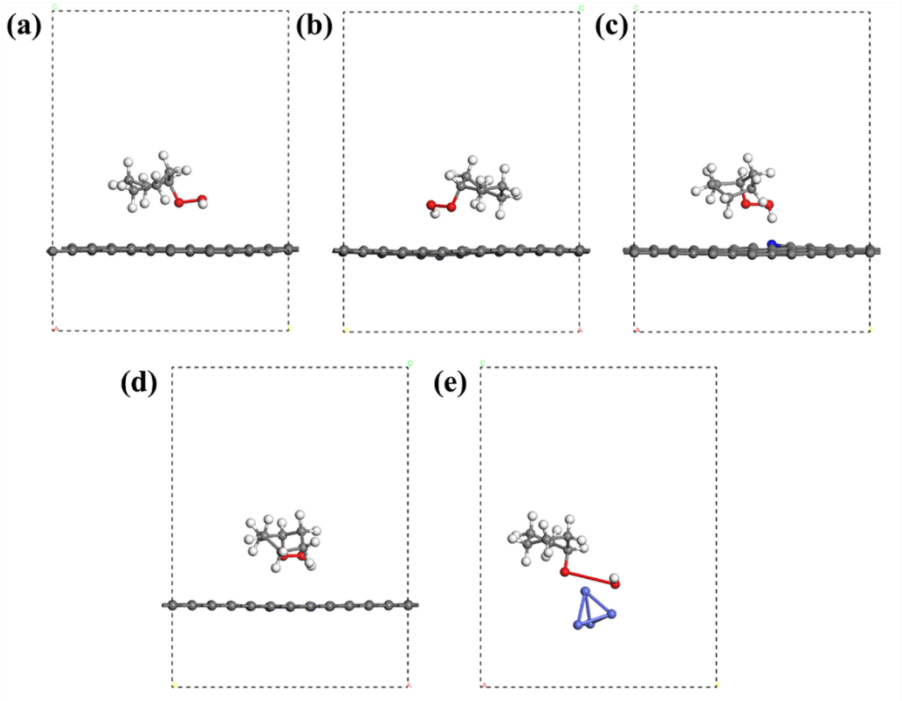


**Figure S8. Side view of the CHHP adsorption on the (a) graphitic-N, (b) pyridinic-N, (c) pyrrolic-N, (d) Co-N-C, (e) $Co_4$.**

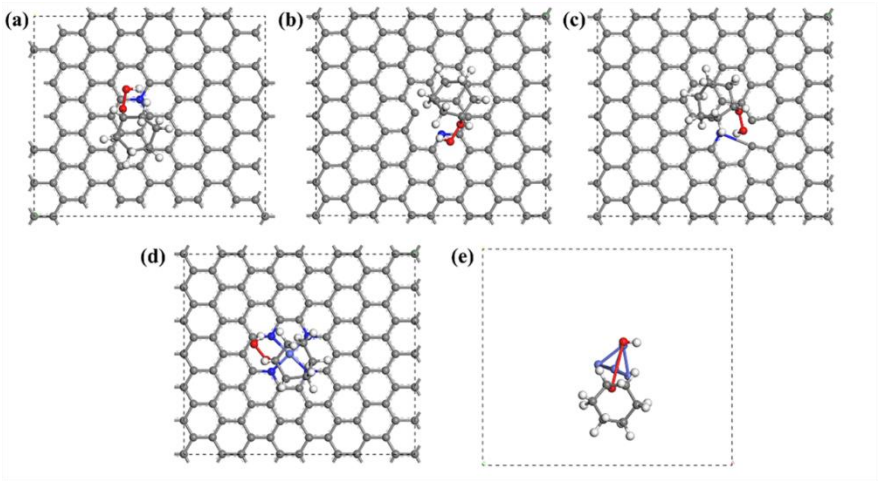


**Figure S9. Top view of the CHHP adsorption on the (a) graphitic-N, (b) pyridinic-N, (c) pyrrolic-N, (d) Co-N-C, (e) $Co_4$.**

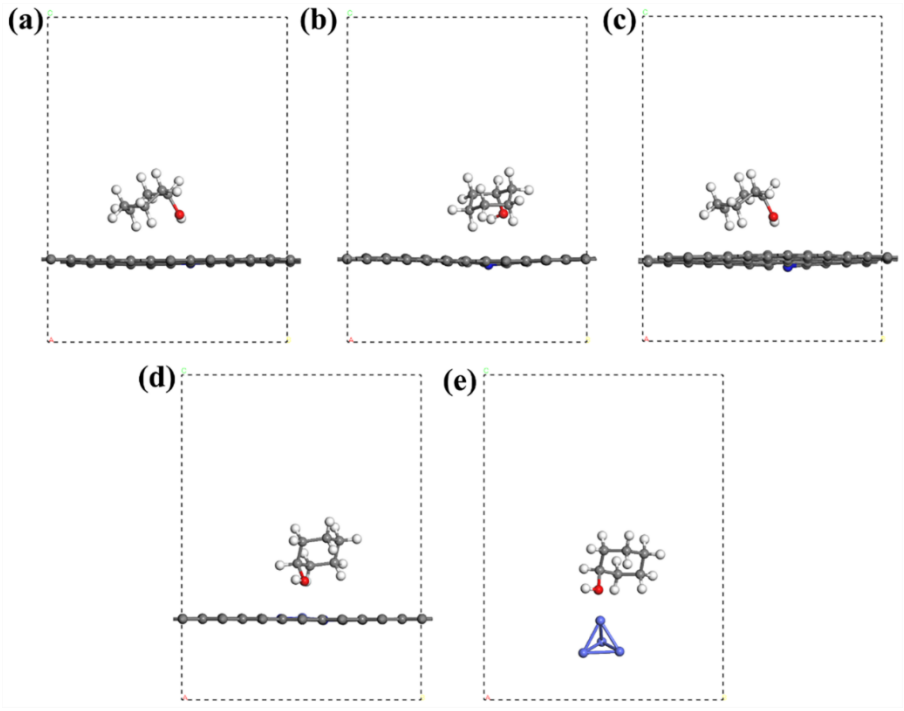


**Figure S10. Side view of the Cy-OH adsorption on the (a) graphitic-N, (b) pyridinic-N, (c) pyrrolic-N, (d) Co-N-C, (e) $Co_4$.**

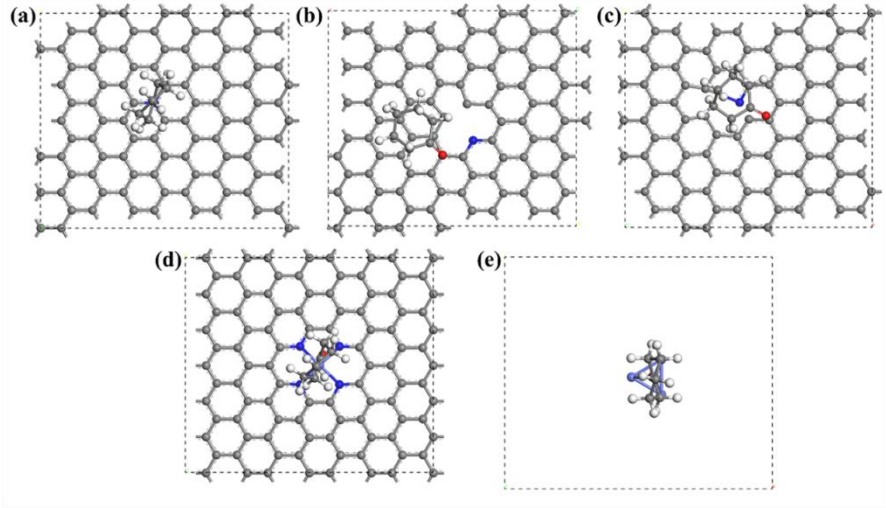


**Figure S11. Top view of the Cy-OH adsorption on the (a) graphitic-N, (b) pyridinic-N, (c) pyrrolic-N, (d) Co-N-C, (e) $Co_4$.**

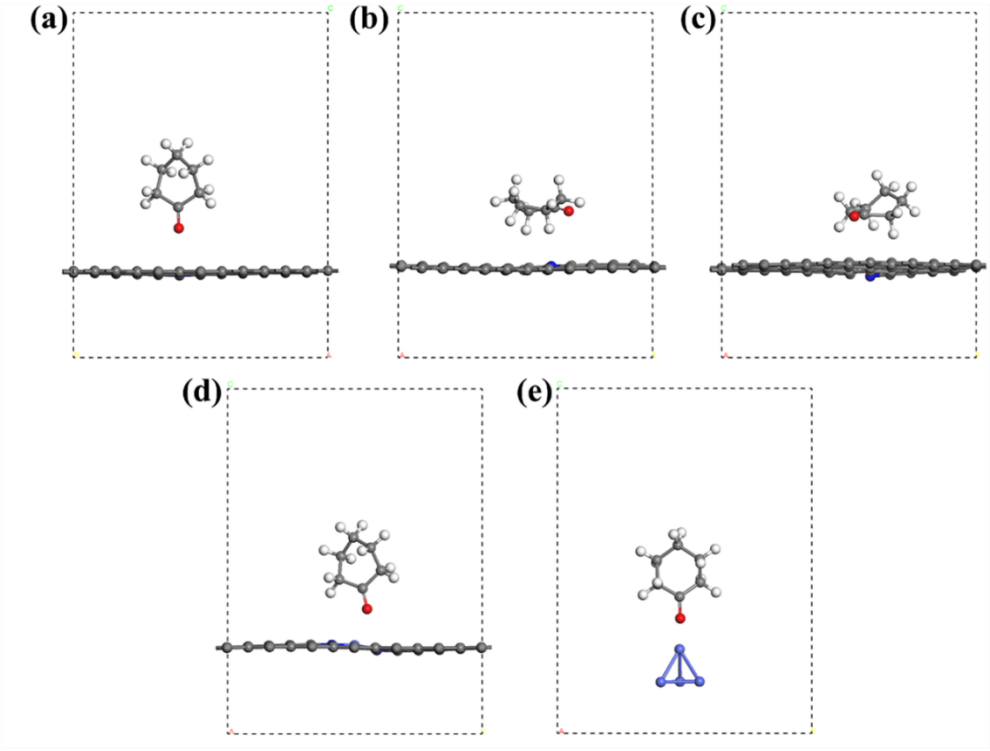


**Figure S12. Top view of the Q=O adsorption on the (a) graphitic-N, (b) pyridinic-N, (c) pyrrolic-N, (d) Co-N-C, (e) $Co_4$.**

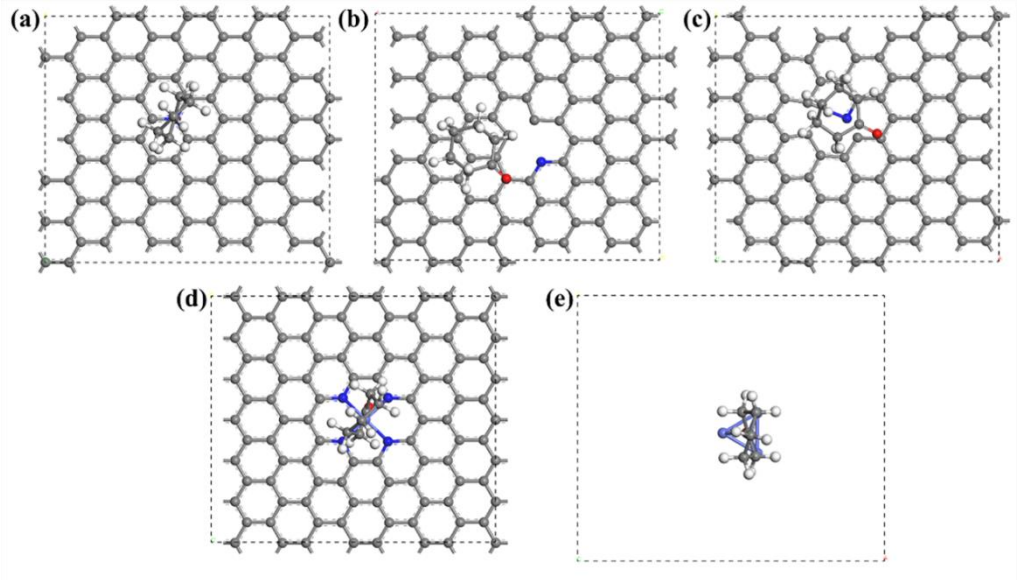


**Figure S13. Top view of the Q=O adsorption on the (a) graphitic-N, (b) pyridinic-N, (c) pyrrolic-N, (d) Co-N-C, (e) $Co_4$.**

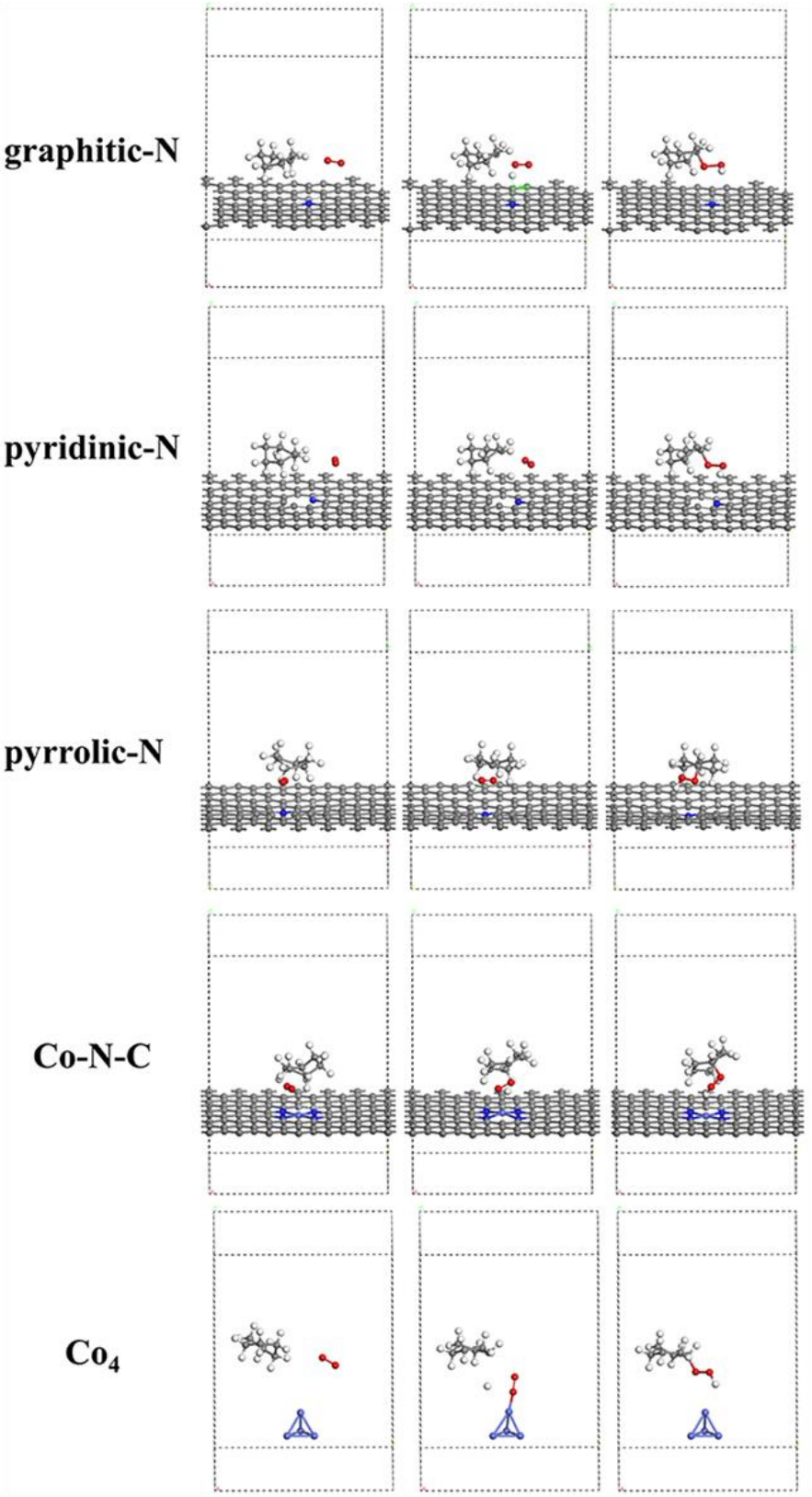


**Figure S14. TS of CHHP on the different active sites.**

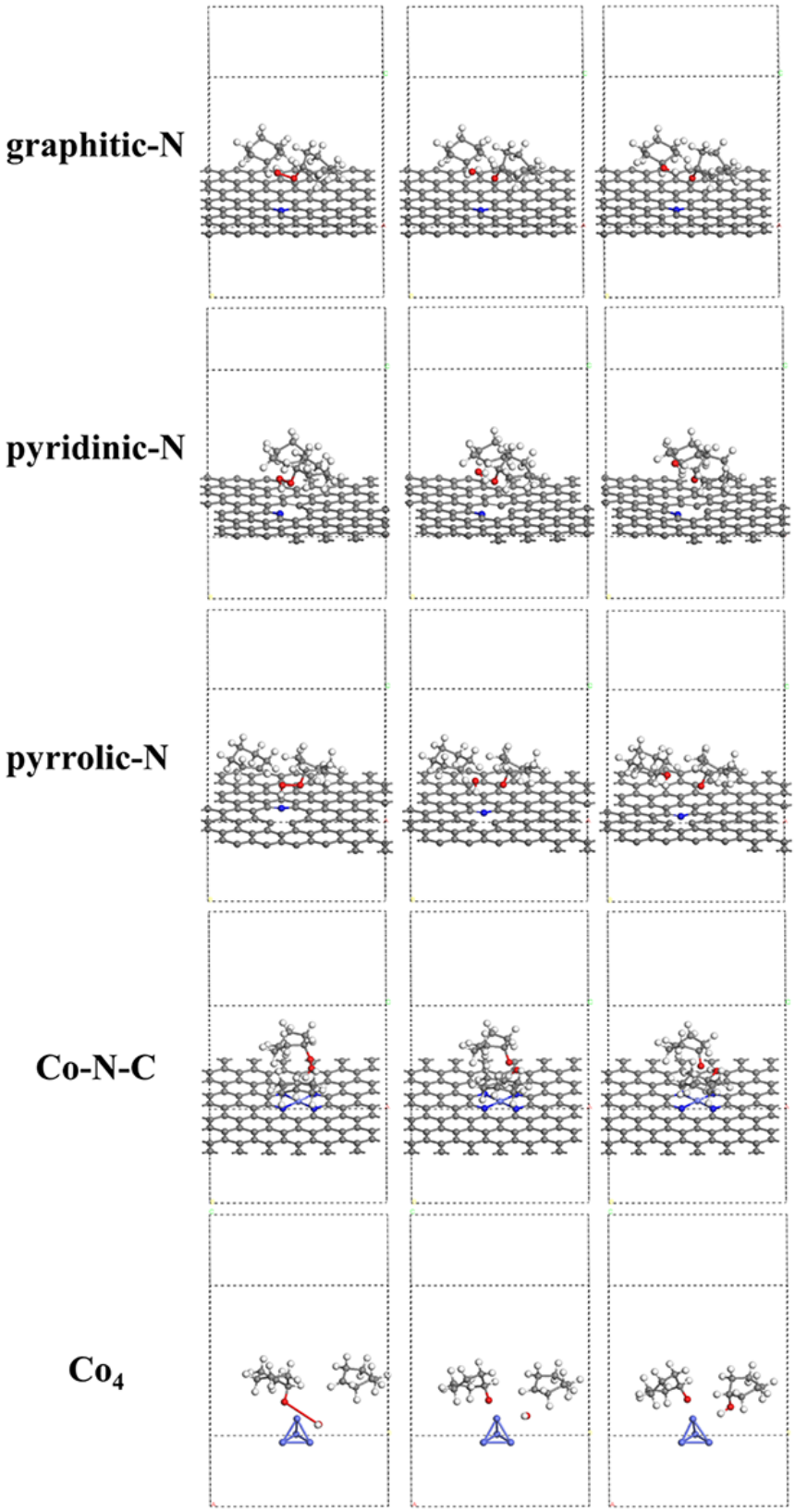


**Figure S15. TS of Cy-OH on the different active sites.**

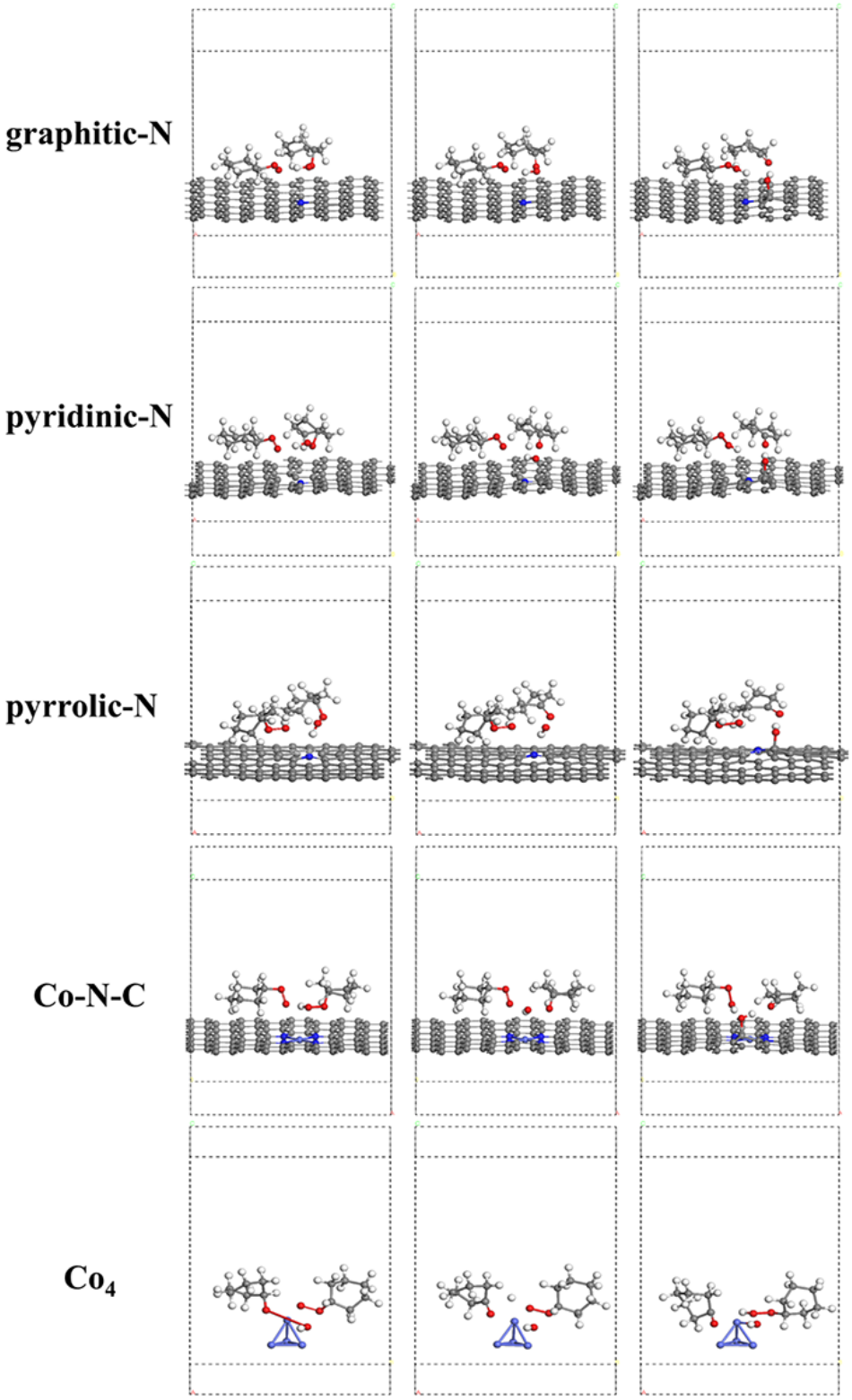


**Figure S16. TS of Q=O on the different active sites.**